Covalent and Reversible Short-Range Electrostatic Imaging in Noncontact Atomic Force Microscopy

Peter Dieška and Ivan Štich

*Center for Computational Materials Science (CCMS), Slovak University of Technology (FEI STU),
Ilkovičova 3, SK-812 19, Bratislava, Slovakia*

Rubén Pérez

Departamento de Física Teórica de la Materia Condensada, Universidad Autónoma de Madrid, E-28049 Madrid, Spain
(Received 2 April 2003; published 18 November 2003)

We present a computational study of atomic-scale image formation in noncontact atomic force microscopy on metallic surfaces. We find two imaging scenarios: (1) atomic resolution arising due to very strong covalent tip-sample interaction exhibiting striking similarity with the imaging mechanism found on semiconductor surfaces, and (2) a completely new mechanism, reversible short-range electrostatic imaging, arising due to subtle charge-transfer interactions. Contrary to the strong covalent-bond imaging, the newly identified mechanism causes only negligible surface perturbation and can account for results recently observed experimentally.

In the past few years frequency modulation (FM) atomic force microscopy (AFM) [1,2](also called noncontact AFM) has developed to a powerful technique for obtaining atomic-scale images of semiconductor [e.g., Si(111) [2], Si(001) [3], polar InP [4,5], GaAs [6], InAs [7]] and insulating surfaces (e.g., alkali halides [8,9]) in UHV. In the FM-AFM technique [10] the cantilever executes large-amplitude oscillations and the surface-related information is inferred from frequency modification (frequency shift) due to tip-surface interaction. Since the first atomic-scale FM-AFM images of Si(111) [2], more systems have been successfully studied. Nevertheless, the number of systems studied with the FM-AFM technique remains limited due, in part, to the fact that the mechanism of atomic-scale resolution of FM-AFM is not completely understood. In spite of the fact that FM-AFM can, at least in principle, be used for atomic-scale imaging of insulating, semiconducting, and metallic surfaces alike, the first application of the technique to metals surfaces has appeared relatively recently. True atomic-scale images of the copper surfaces have been presented by Loppacher *et al.* [11,12] and of Ag(111) by Orisaka *et al.* [13]. The importance of imaging the metal surfaces with FM-AFM is primarily in their combination with simultaneous scanning tunneling microscopy (STM) image collection with the two techniques offering complementary information.

In order to use the FM-AFM technique routinely to a wide range of systems, a theoretical model is required that allows interpretation of the experimental images. Theory has provided very strong indication that on reactive semiconductor surfaces the short-range chemical tip-surface interaction significantly enhances the atomic resolution of the FM-AFM [14–18]. This interaction can be thought of as dangling bond-dangling bond type of interaction [15]. Experiments have shown that the observed image reflects variation of local reactivity between the tip and the sample [19–23] and thus have corroborated the theoretical predictions. On the other hand, on ionic surfaces, such as NaCl, MgO, or LiF, the atomic resolution has been shown to arise primarily due to short-range electrostatic interactions [24]. Imaging metals with any scanning probe (even STM) is challenging because of the short interatomic distances and low charge corrugation. It is then a test of the resolution capabilities of the FM-AFM. On metallic surfaces the situation is expected to be different from the two above mentioned scenarios. The delocalized nature of valence electronic charge on metals surfaces is less likely to lead to the spatially very localized tip-surface interaction, which was behind the atomic resolution on semiconductor surfaces and for the same reason is unlikely to lead to spatial variation of electrostatic potential across the surface, as was the case on alkali halide surfaces. These arguments seem to suggest that a completely different mechanism and model need to be evoked for understanding FM-AFM results for each of the three groups of surfaces. To the best of our knowledge, unlike for semiconductors and insulators where studies and models are already readily available, no realistic atomistic study of the FM-AFM imaging mechanism exists for metallic surfaces.

One might hope to benefit from the experience acquired in understanding the STM images of related metals surfaces. Unfortunately, even here the situation is not fully understood. In order to explain the first measured STM images of (111) surfaces of Au and Al [25,26], special tip induced effects had to be invoked [27]. The recent combined dynamic FM-AFM/STM experiments [12] on Cu surfaces contributed further puzzles. They yield images with atomic resolution but with estimated chemical forces about an order of magnitude smaller than expected and decay length factors for tunneling currents

(λ_T) and tip-surface forces (λ_F) about a factor of 3 larger than expected and $\lambda_F = 2\lambda_T$. These experimental findings call for a clear understanding of the mechanism behind the observed atomic resolution imaging on metallic surfaces.

To this point we use a case study, Cu(001) surface [11,12], to conduct a search for the imaging mechanism. Our main finding is that the most common way the tip interacts with a metallic surface is again a very strong, spatially localized covalent bond, very closely mimicking the scenario found on semiconducting surfaces. However, the existing experimental results [11,12] can be accounted for only by assuming the presence of another, much weaker type of tip-surface force, arising from reversible charge-transfer processes between the tip and the metal surface. A brief account of some aspects of the present work was presented in [28].

Our model for the tip-surface interaction is based on division [14,15,24] of the tip into a macroscopic part which contributes mainly the long-range background interaction, such as van der Waals, and a nanotip which is responsible for short-range forces. The background long-range interactions depend on the details of the tip, which can be taken from experiments [29]. Si tips have been used in the experiments [11,12]. We model the nanotermination of the tip by a small (four-atom) Si nanoasperity saturated at the base by H atoms [14,15]. The main characteristics of such a Si nanotip is the presence of one singly occupied dangling bond sticking out of the tip apex. The dangling bond was found instrumental for atomic resolution of FM-AFM on reactive surfaces [14,15]. We also consider other tip terminations, which may result from contamination by impurities from the vacuum chamber or surface material. We use a four (double) layer thick slab model with a 3×3 surface unit cell to describe the surface. In the z direction the periodic images were separated by a vacuum region. The calculation of the tip-surface force versus distance curves is performed by stepwise displacements of the model tip towards the surface. At each tip position the structure of the interacting tip-surface system is relaxed, and the tip-surface force calculated. In the structural relaxation the tip base with the H saturation as well as the atoms in the bottom surface layer are kept fixed to emulate the proper tip/surface termination. The normal force acting on the tip is calculated as a numerical derivative of the energy curve. We consider no applied voltage [30]. The energies and forces were calculated within the density functional theory in its plane-wave pseudopotential formulation [31] using the CASTEP suite of codes [32]. All atoms were described by ultrasoft pseudopotentials [33]. We use gradient corrected functional for the exchange-correlation energy [35]. The wave fuctions were expanded on a mesh of two Monkhorst-Pack k points [36] with a plane-wave cutoff of 270 eV. A smearing width of $\sigma = 0.2$ eV was used [37]. Standard tests show that this set of parameters provides a very accurate description of the system. We

have found that a dipole is formed when the tip approaches the surface. However, the change of the dipole moment as a function of the tip-surface distance is negligible. Hence, the results are not affected by spurious dipole image interactions [38].

Our results for vertical scans over on-top and hollow sites of the Cu(001) surface with a pure Si tip are shown in Fig. 1(a). The magnitude and range of the tip-surface forces (≈ 2 nN, 3 Å) and interaction energies (≈ 2 eV) are characteristic of a strong covalent bond. This striking result is further depicted in Fig. 2 by comparing the interaction of the Si tip with the Cu(001) surface with that of a reactive semiconductor surface with the two
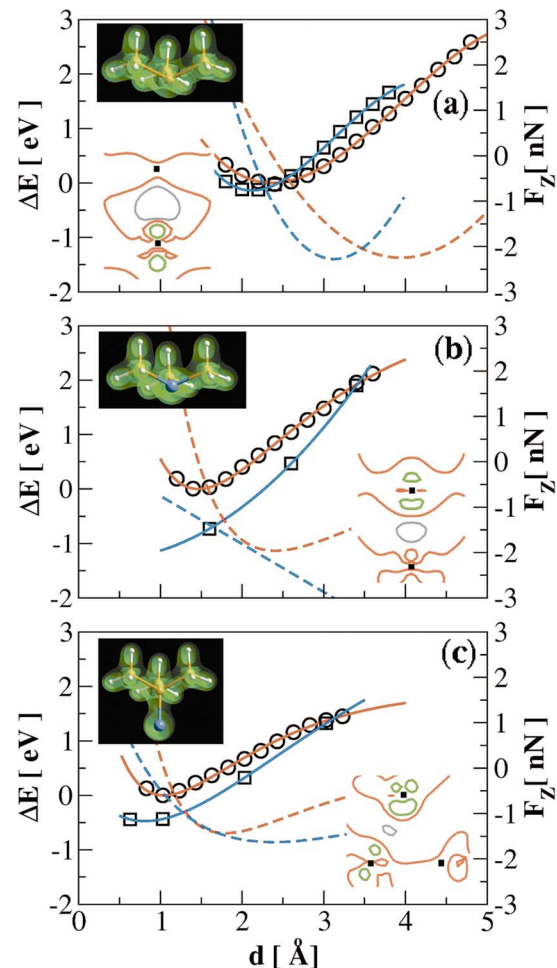

FIG. 1 (color). Scans of short-range tip-surface energy over on-top (red color, circles) and hollow sites (blue color, boxes) and normal force (red and blue broken lines). Solid lines in energy curves are fits to the computed data. (a) Scans with pure Si tip, (b) Si tip terminated by Cu apex, and (c) Si tip terminated by Cu impurity removed from the surface. The minimum of the energy curves over on-top sites is taken as zero. The insets show the tips with two typical isosurfaces of constant (valence) electronic charge density and induced charge densities [$\rho(\mathbf{r})_{\text{tip-sample}} - \rho(\mathbf{r})_{\text{tip}} - \rho(\mathbf{r})_{\text{sample}}$] around the apex/scanned atom (black boxes) due to tip-sample interaction (red zero, black charge pileup, green charge depletion).
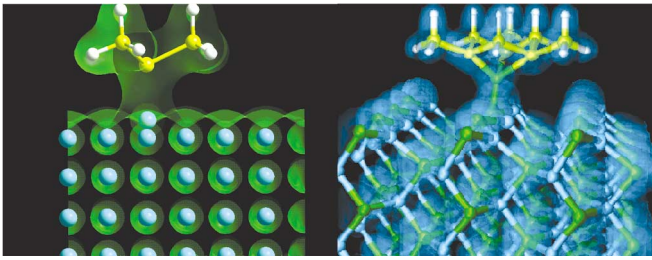
FIG. 2 (color). Chemical bond between Cu(001) surface and a pure Si tip (left) compared with bonding on an InP(110) surface.

interactions being almost indistinguishable. Hence, despite the more delocalized reactive charge, a very well localized covalent bond between the tip and the metal surface is formed. This covalent bond is formed by populating the bonding state formed from a singly occupied apex dangling bond with charge removed from the scanned atom underneath the tip. At variance with semiconducting surfaces where the tip was primarily reacting with the dangling bonds on the surface atoms, on the metal surface the minimum of the energy is over the hollow site. One consequence of this bonding situation is that, in the on-top position, there is a large surface response with the surface Cu atom so strongly bonded to the tip that it follows the apex (Fig. 2). This ultimately leads to creation of a vacancy and modification of the tip apex. Hence, this tip-surface interaction would not lead to a stable imaging with the atomic resolution found in the experiments [11,12]. Similarly, the strength of the computed force and its range are both incompatible with the results measured in the experiments [12]. A better insight may be gained from a computer graphics animation [39]. We note that the extraction of a surface atom may be even more likely from other surfaces, e.g., gold. This gives further support to the suggestions made in connection with explanation of the STM images of metals [27].

In the effort to shed light on the observed imaging mechanism, we consider other probable tip apex configurations. Apex modifications are very likely to occur because of contamination or tip instability. Two such examples are shown in Figs. 1(b) and 1(c). The first tip has a Cu atom built into the Si tip as an apex. Such an apex may form from a tip crash into the surface. The other tip has an apex formed by a Cu atom removed from the surface and bonded to the Si apex. Such an apex will readily form on Cu surfaces. The results shown in Figs. 1(b) and 1(c) indicate that none of the two tips would remove the imaged Cu atom from the surface in line with the reduced amount of induced charge and weaker tip-sample interaction energy. Both apexes should provide a rather stable imaging, albeit with hollow sites appearing as protrusions. The apex with the Cu atom removed from the surface appears to be more compliant. On approach the Cu apex deforms and forms inequivalent bonds to two adjacent surface atoms [cf. Fig. 1(c)]. Despite providing

stable imaging, both types of tip-surface interactions correspond to strong imaging, which cannot account for the experimentally determined chemical interaction.

The measured short-range forces indicate that the imaging was not done using covalent tip-surface forces. Based on resistance measurements [12], existence of a thin oxide layer on the tip can be assumed. This situation represents a very complex tip termination. We use the simplest, yet realistic model to describe the tip termination, namely, a H_2O molecule. The H termination mimics the local chemistry of the O apex in the oxide layer. The results, shown in Fig. 3, are interesting also because oxidized tips are commonly used in FM-AFM. Given the simplicity of the model, the calculated results are in decent agreement with experiments. While the range of the calculated force is shorter than in the experiment, its strength is in the experimental range. A more realistic tip termination with more O atoms interacting with the surface, as well as a more realistic treatment of the dispersive interactions, would cause a convolution of the curve and further improve the agreement with experiment. Interaction of H_2O with metal surfaces is not entirely understood [40]. The weak interaction results from three types of interactions: (1) van der Waals, (2) dipole-dipole, (3) charge transfer. Of these, the last one is generally the strongest. The strength of this interaction critically depends on the ionization potential of the tip and the electron affinity of the metal. In the present model, the ionization potential of water is very high and resulting from the lone-pair orbital of water. Therefore, the net effect of the electric field due to the reversible charge transfer between the tip and the surface (Fig. 3) is weak. This imaging mechanism is very different from the other mechanisms identified here or on semiconductor surfaces [14]. As shown in Fig. 1, in those cases an induced charge pileup occurs between the tip and the surface atom(s) whose amount determines the strength of the tip-surface interaction. The bonding of the model water tip, analyzed in Fig. 3, shows that the tip-surface overlap is extremely weak. Because of the large ionization potential of water, the situation is only marginally altered if a more favorable orientation of the lone-pair orbital to the surface is considered (not shown). This provides an explanation for the experimentally found, but not fully understood, relation $\lambda_F = 2\lambda_T$ [12] between the force and tunneling current decay lengths. Such a relation has been proposed by Chen [41] assuming weak electronic tip-surface overlap. We note that tip adsorbed water, a common contaminant, could provide a similar imaging mechanism. Use of this weak imaging, where possible, has the advantage over the strong imaging of perturbing only negligibly the sample. We expect this imaging to work equally well on reactive semiconductor surfaces.

In conclusion, we have performed the first simulation of the FM-AFM image formation on metallic surfaces. We find that the most natural tip terminations yield very
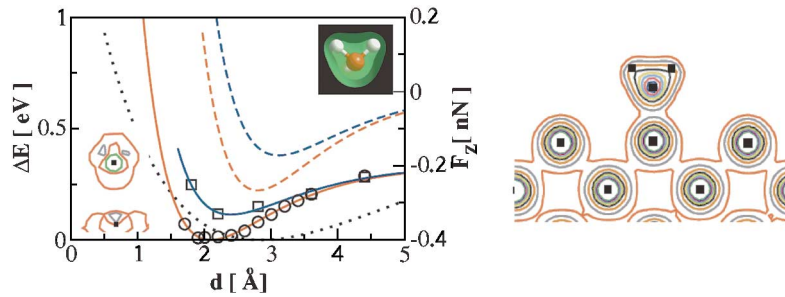
FIG. 3 (color). Results for model H_2O tip. Left panel: vertical scans. Labeling of the curves and insets as in Fig. 1. The dotted curve shows the experimentally determined chemical force [12] with minimum shifted horizontally to coincide with the position in the computed curves. Right panel: total (valence) charge density for the H_2O model tip.

strong covalent tip-surface interaction, indistinguishable from that typically found on semiconductor surfaces. Hence, atomic-scale imaging for both types of material may result from the same mechanism of a strong covalent tip-surface interaction. Completely different stable imaging was found to result from weak reversible short-range electrostatic charge-transfer imaging, which, in turn, provides explanation for the experimentally observed double decay length for AFM, compared to STM. Apex engineering, assisted by computer modeling, may help to optimize the imaging mechanism by identifying tip terminations, maximizing surface corrugation while simultaneously minimizing perturbation to the measured surface and formation of unstable tips.

[1] F. J. Giessibl, Jpn. J. Appl. Phys. **33**, 3726 (1994).
[2] F. J. Giessibl, Science **267**, 68 (1995).
[3] S. Kitamura and M. Iwatsuki, Jpn. J. Appl. Phys. **35**, L668 (1996).
[4] Y. Sugawara et al., Science **270**, 1646 (1995).
[5] H. Ueyama et al., Jpn. J. Appl. Phys. **34**, L1086 (1995).
[6] M. Ohta et al., J. Vac. Sci. Technol. B **13**, 11 265 (1995).
[7] A. Schwarz et al., Appl. Surf. Sci. **140**, 293 (1999).
[8] M. Bammerlin et al., Probe Microsc. **1**, 3 (1997).
[9] S. P. Jarvis et al., Nature (London) **384**, 247 (1996).
[10] R. Garcia and R. Perez, Surf. Sci. Rep. **47**, 197 (2002).
[11] Ch. Loppacher et al., Appl. Surf. Sci. **140**, 287 (1999).
[12] Ch. Loppacher et al., Phys. Rev. B **62**, 16 944 (2000).
[13] S. Orisaka et al., Appl. Surf. Sci. **140**, 243 (1999).
[14] R. Pérez, M. C. Payne, I. Štich, and K. Terakura, Phys. Rev. Lett. **78**, 678 (1997).
[15] R. Pérez, I. Štich, M. C. Payne, and K. Terakura, Phys. Rev. B **58**, 10 835 (1998).
[16] S. H. Ke, T. Uda, R. Pérez, I. Štich, and K. Terakura, Phys. Rev. B **60**, 11 631 (1999).
[17] J. Tóbik, I. Štich, R. Pérez, and K. Terakura, Phys. Rev. B **60**, 11 639 (1999).
[18] J. Tóbik, I. Štich, and K. Terakura, Phys. Rev. B **63**, 245324 (2001).
[19] T. Uchihashi et al., Phys. Rev. B **56**, 9834 (1997).
[20] R. Erlandsson, L. Olsson, and P. Mårtenson, Phys. Rev. B **54**, R8309 (1996).
[21] M. A. Lantz et al., Phys. Rev. Lett. **84**, 2642 (2000).
[22] M. A. Lantz et al., Science **291**, 2580 (2001).
[23] T. Eguchi and Y. Hasegawa, Phys. Rev. Lett. **89**, 266105 (2002).
[24] A. I. Livshits, A. L. Schluger, A. L. Rohl, and A. S. Foster, Phys. Rev. B **59**, 2436 (1999).
[25] V. M. Hallmark et al., Phys. Rev. Lett. **59**, 2879 (1987).
[26] J. Wintterlin et al., Phys. Rev. Lett. **62**, 59 (1989).
[27] S. Ciraci et al., Phys. Rev. B **46**, 10 411 (1992).
[28] I. Štich, P. Dieška, and R. Pérez, Appl. Surf. Sci. **188**, 325 (2002).
[29] M. Guggisberg et al., Phys. Rev. B **61**, 11 151 (2000).
[30] S.-H. Ke, T. Uda, and K. Terakura, Phys. Rev. B **65**, 125417 (2002).
[31] See, for instance, M. C. Payne et al., Rev. Mod. Phys. **64**, 1045 (1992).
[32] We used a CASTEP 4.2 (academic version) suite of programs; for the theory behind this code see Refs. [31,33,34].
[33] D. Vanderbilt, Phys. Rev. B **41**, 7892 (1990).
[34] G. Kresse and J. Furthmüller, Phys. Rev. B **54**, 11 169 (1996); D. R. Bowler and M. J. Gillan, Chem. Phys. Lett. **325**, 473 (2000).
[35] J. P. Perdew et al., Phys. Rev. B **46**, 6671 (1992).
[36] H. J. Monkhorst and J. D. Pack, Phys. Rev. B **13**, 5188 (1976).
[37] M. J. Gillan, J. Phys. Condens. Matter **1**, 689 (1989).
[38] M. R. Jarvis et al., Phys. Rev. B **56**, 14 972 (1997).
[39] A computer graphics animation of the simulation can be downloaded from http://www.ccms.elf.stuba.sk/ra_afm.html.
[40] M. A. Henderson, Surf. Sci. Rep. **46**, 1 (2002).
[41] C. J. Chen, *Introduction to Scanning Tunneling Microscopy* (Oxford University Press, New York, 1992), Chap. 7.